Simultaneous Dual-Parameter Measurement Based on a Modified Vernier Effect at the Equal-FSR Critical Condition

Yunqing Guan, Matthias Fabian, Dongsheng Wu, Yingbin Feng, Hongwei Gao, Tong Sun and Kenneth T. V. Grattan

***Abstract*—This work both investigates the critical state of the Vernier effect scheme in which the interferometric spectra of the sensing interferometer and the reference interferometer attain equal free spectral ranges (FSRs) at a specific wavelength, and then explores how the zero point of the FSR-difference curve can be used to determine the unique wavelength (UWL) of the Vernier envelope. The analysis carried out has revealed a new mechanism for realizing dual-parameter measurement. Furthermore, building on this, a compact sensing scheme has then been proposed as a proof of the concept, where this mechanism has been verified using only a single sensing interferometer. By selecting the central wavelength of the measurement range as the turning point and generating an inverted spectrum of the sensing spectrum as the reference, the resulting output Vernier envelope features a UWL. This positive approach introduces a uniquely identifiable wavelength in the conventional Vernier envelope and enables dual-parameter sensing by simultaneously tracking the UWL intensity variation and the wavelength shift of the peak or dip adjacent to the UWL. The effectiveness of the proposed scheme has then been experimentally validated through temperature and humidity measurements, as exemplars. The investigation of the critical FSR-equality condition thus provides new insights for increasing the number of measurable parameters, thereby offering a promising pathway towards novel Vernier schemes with distinctive spectral characteristics and enhanced capabilities for multi-parameter measurement.**

***Index Terms*—Vernier effect, unique wavelength, equal FSRs, dual-parameter measurement.**

I. INTRODUCTION

WITH the growing demand for high-sensitivity sensing technologies, the optical Vernier effect has attracted considerable attention in recent years. Originating from the well-known working principle of the Vernier caliper, the traditional Vernier effect scheme employs two interferometers, one serving as the sensing interferometer and the other as a reference. These interferometers are designed with closely matched FSRs, where only the sensing interferometer responds to variations in the measurand, while the reference interferometer remains stable throughout the measurement process [1], [2], [3]. By cascading (or paralleling) the two interferometers, a periodic Vernier envelope can be extracted by fitting the peaks or the dips of the output spectrum. Compared with the direct response of a single sensing interferometer to the measurand, using the Vernier envelope offers significantly amplified sensitivity. Building on this advantage, Vernier effect-based sensing schemes have been successfully demonstrated in fields such as industrial monitoring [4], [5], [6], healthcare diagnostics [7], [8], [9], environmental detection [10], [11], [12], and various other application areas.

However, precisely satisfying the FSR matching condition between the sensing and reference interferometers, as well as maintaining a stable reference interferometer, is challenging in practice. To address this issue, the computational Vernier effect has been widely reported in the literature [13], [14], including in our previous work [15], where a virtual reference interferometer is digitally constructed and flexibly adjusted to achieve the desired FSR matching condition, thereby enabling cost-effective sensitivity enhancement. Nevertheless, the resulting Vernier envelope is inherently periodic because the two interferometers themselves exhibit periodic spectral characteristics, making it difficult to track a specific peak or dip wavelength during long-term or even continuous measurements. In addition, multiple wavelengths within the envelope tend to respond similarly to variations in the measurand, which fundamentally limits the ability of the scheme to achieve reliable dual-parameter measurements. Most importantly, the existing Vernier effect schemes rely exclusively on interferometers with slightly different, i.e. in practice non-identical FSRs, leaving the critical condition of exact FSR equality unexplored. This gap restricts the deeper understanding of the underlying spectral behavior and limits the potential to unlock new sensing functionalities.

This work was supported by the basic scientific research project of Liaoning Provincial Department of Education (Grant Number: LJ212410144058), the Doctoral Research Initiation Project under the Liaoning Provincial Natural Science Foundation (Grant Number: 2025-BS-0341), the Postdoctoral Program under the China Scholarship Council, the Joint Program Project under the Liaoning Provincial Science and Technology Plan (Grant Number: 2025110676-JH4/4800), the Joint Program Project under the Liaoning Provincial Science and Technology Plan (Grant Number: 2025JH2/101800399). (*Corresponding authors: Yunqing Guan, Yingbin Feng, Hongwei Gao.*)

Yunqing Guan, Dongsheng Wu and Yingbin Feng are with the School of A utomation and Electrical Engineering, Shenyang Ligong University, Shenyang 110159, China. (e-mail: yunqingguan@sylu.edu.cn; wuds@sylu.edu.cn; sylg_fyb@sylu.edu.cn).

Hongwei Gao is with the Institute of International Engineering, Shenyang Ligong University, Shenyang 110159, China. (e-mail: ghw1978@sylu.edu.cn)

Matthias Fabian, Tong Sun and Kenneth T. V. Grattan are with the School of Science and Technology, City St George's, University of London, London E C1V 0HB, U.K.(e-mail: matthias.fabian.1@city.ac.uk; T.Sun@citystgeorges.a c.uk; K.T.V.Grattan@citystgeorges.ac.uk).

Building on early studies of a special type of modal interferometer by the authors, it has been demonstrated here that by introducing a characteristic wavelength, this disrupts the inherent spectral periodicity and enables the simultaneous measurement of multiple parameters [16], [17], [18]. This characteristic wavelength emerges when the wavelength derivative of the propagation constant difference between the two interfering modes, $\frac{d\Delta\beta}{d\lambda}$, approaches zero, under which condition the corresponding FSR tends toward infinity. Inspired by this mechanism, it is hypothesized that a similar principle can be extended to the Vernier effect. Specifically, when the FSRs of the two interferometers are designed to be equal (within the particular wavelength region), a zero point appears in the FSR difference curve, causing the FSRs of the Vernier envelope to diverge. Under this condition, unique spectral features, such as a distinguishable wavelength, can emerge in the resulting Vernier envelope. Such features can then positively facilitate high-sensitivity and dual-parameter sensing. Therefore, understanding the relationship between the UWL within the Vernier envelope and the zero point of the FSR difference curve constitutes a key scientific question that warrants the in-depth investigation in this paper. Nevertheless, studying the critical condition of equal FSRs remains challenging, primarily because the FSR of an interferometer typically increases monotonically with wavelength. As a result, it is generally difficult for two different interferometers to exhibit identical FSRs within the same wavelength region.

To address the limitation of conventional Vernier effect-based sensors, namely the strict requirement of precise FSR matching, and to enable high-sensitivity dual-parameter measurement, this work investigates the previously unexplored equal-FSR critical condition. A novel sensing strategy is proposed in which a UWL is introduced from the interferometric spectrum into the Vernier envelope. The proposed design requires only one sensing interferometer, and the corresponding reference spectrum has been obtained by overturning the sensing spectrum along the wavelength axis using the midpoint of the overall measurement wavelength range, i.e. λ_0, as the overturn point. The UWL can be seen to emerge precisely at the overturned wavelength λ_0, enabling an experimental demonstration of simultaneous humidity and temperature measurement by tracking the UWL intensity and wavelength shift of the nearby peak. In a way that is distinct from conventional Vernier effect schemes, the introduction of the UWL fundamentally breaks the absolute periodicity of the traditional Vernier envelope, giving rise to a quasi-periodic spectral feature with distinctive evolution characteristics, enabling simultaneous dual-parameter measurement with high sensitivities. To the best of our knowledge, this is the first study that not only elucidates the equal-FSR critical condition, but also reveals the physical mechanism of UWL generation within the Vernier envelope, thereby establishing a new paradigm for breaking absolute periodic constraints and achieving high-performance dual-parameter sensing.

II. Principle, Analysis and Theoretical Simulation

A. Reference Analysis of the Infinite-FSR Phenomenon in a Special Two-Mode Interferometer

For a conventional modal interferometer based on the Mach-Zehnder configuration, two light waves propagating through a homogeneous medium meet and interfere at the output. The resulting phase difference $\Delta\varphi$ can be expressed as:

$$\Delta\varphi = \Delta\beta L \tag{1}$$

where $\Delta\beta$ denotes the propagation-constant difference between the two interfering modes and L is the propagation length. Both $\Delta\varphi$ and $\Delta\beta$ are functions of the wavelength used, λ.

The FSR is generally defined as the wavelength interval between two adjacent peaks or dips in the interferometric spectrum. Consequently, for two adjacent spectral extrema at λ_0 and $\lambda_0 + FSR$, the phase difference fulfills the following:

$$|\Delta\varphi(\lambda_0 + FSR) - \Delta\varphi(\lambda_0)| = 2\pi \tag{2}$$

Generally, $\Delta\varphi(\lambda)$ is a smooth and differentiable function of wavelength. Therefore, a first-order Taylor expansion of $\Delta\varphi(\lambda_0 + FSR)$ around λ_0 yields:

$$\Delta\varphi(\lambda_0 + FSR) \approx \Delta\varphi(\lambda_0) + \frac{d\Delta\varphi(\lambda_0)}{d\lambda} FSR \tag{3}$$

By solving equation (2) and equation (3) simultaneously, the relationship between the FSR and the $\frac{d\Delta\beta(\lambda_0)}{d\lambda}$ can be obtained as:

$$FSR = \frac{2\pi}{\left|\frac{d\Delta\varphi(\lambda_0)}{d\lambda}\right|} = \frac{2\pi}{L\left|\frac{d\Delta\beta(\lambda_0)}{d\lambda}\right|} \tag{4}$$

For a conventional interferometer, $\Delta\beta(\lambda)$ typically varies monotonically with λ. As a result, the FSR also changes monotonically with λ, leading to an inherently periodic interferometric spectrum. However, such a periodic spectrum lacks distinctive and uniquely identifiable peaks or dips, making it difficult to reliably track a specific spectral feature, particularly in long-term or continuous measurements. Moreover, this intrinsic periodicity fundamentally limits the ability to realize robust dual-parameter sensing.

To overcome these limitations, previous work undertaken by the authors investigated a special interferometer that exhibits a characteristic wavelength (CWL) in its spectrum, enabling simultaneous multi-parameter measurement [19], [20]. The emergence of this characteristic wavelength originates from a deliberate refractive-index design of the fiber, which introduces an extreme point in the propagation-constant curve $\Delta\beta(\lambda)$. Furthermore, according to equation (4), when $\frac{d\Delta\beta(\lambda)}{d\lambda}$ approaches zero at CWL, the corresponding FSR becomes nonmonotonic and tends to diverge. Under this condition, the interference intensity no longer exhibits a periodic variation with wavelength in the vicinity of CWL. This phenomenon gives rise to the CWL in the spectrum and forms the physical basis for dual-parameter detection.

B. Critical Condition for the Infinite-FSR Phenomenon of a Vernier Effect Scheme

The conventional Vernier effect scheme consists of a sensing interferometer and a reference interferometer with closely matched FSRs. As an example, both interferometers are configured as Fabry-Perot cavities and arranged in parallel. The resulting output spectral intensity I can be expressed as:

$$I = I_R + I_S = 4I_0 + 2I_0 \cos\Delta\varphi_R + 2I_0 \cos\Delta\varphi_S \quad (5)$$

where I_R and I_S denote the spectral intensities of the reference and the sensing interferometers, respectively. To facilitate the derivation, the intensities of the two interfering light waves within each interferometer have been considered equal, with their common value denoted by I_0. The terms $\Delta\varphi_R$ and $\Delta\varphi_S$ correspond to the phase differences of the reference and the sensing interferometers, respectively. After simplification, the AC component of the output, I_{ac}, can be written as:

$$\begin{aligned} I_{ac} &= 2I_0\left(\cos\frac{4\pi n_R L_R}{\lambda} + \cos\frac{4\pi n_S L_S}{\lambda}\right) \\ &= 2\cos\frac{2\pi\left(n_S L_S - n_R L_R\right)}{\lambda}\cos\frac{2\pi\left(n_S L_S + n_R L_R\right)}{\lambda} \end{aligned} \quad (6)$$

where n_R and n_S denote the refractive indices of the transmission media in the reference and sensing interferometers, respectively, while L_R and L_S represent the cavity lengths of the reference and sensing interferometers. I_{ac} can be further expressed as the product of a low-frequency term, $2cos\frac{2\pi(n_S L_S - n_R L_R)}{\lambda}$ and a high-frequency term, $cos\frac{2\pi(n_S L_S + n_R L_R)}{\lambda}$.

As shown by the red dots in Fig. 1, the upper Vernier envelope of the output spectrum can be extracted by fitting the maxima of the high-frequency component. The obtained Vernier envelope exhibits a profile similar to that of a single interferometer and likewise presents a periodic characteristic. Accordingly, in a way analogous to the FSR of a single interferometer, the free spectral range of the Vernier envelope, denoted as FSR_E, is defined as the wavelength spacing between two adjacent peaks or valleys of the spectral envelope, as illustrated in Fig. 1.

Since the period of the Vernier envelope corresponds to half that of the low-frequency component, the phase difference between two adjacent envelope maxima in the low-frequency term is π, leading to the following condition:

$$\left|\frac{2\pi\left(n_S L_S - n_R L_R\right)}{\lambda_{E1}} - \frac{2\pi\left(n_S L_S - n_R L_R\right)}{\lambda_{E2}}\right| = \pi \quad (7)$$

where λ_{E1} and λ_{E2} are the wavelengths of two adjacent envelope peaks as shown in Fig. 1.

Consequently, FSR_E can be expressed as [21], [22]:

$$\begin{aligned} FSR_E &= \left|\lambda_{E2} - \lambda_{E1}\right| = \frac{\lambda_{E1}\lambda_{E2}}{\left|2\left(n_S L_S - n_R L_R\right)\right|} = \frac{FSR_S FSR_R}{\left|\Delta FSR\right|}, \\ \Delta FSR &= FSR_S - FSR_R \end{aligned} \quad (8)$$

where FSR_S and FSR_R denote the FSR of the sensing and reference interferometers, respectively, and ΔFSR represents the difference between them.

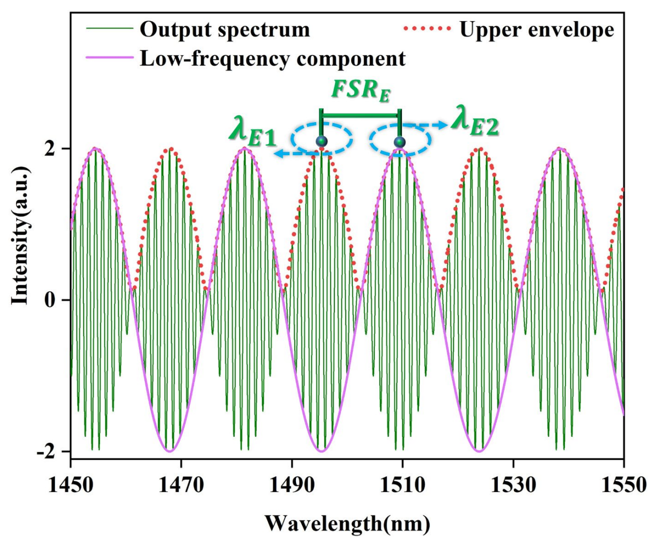

Fig. 1. Simulated curves of the output spectrum and Vernier envelope. (Parameters: $n_R = n_S$=1, L_S=800 μm, L_R=880 μm)

Borrowing the analysis of equation (4) for the FSR of a single interferometric spectrum, the emergence of a CWL requires the FSR to diverge in a specific wavelength region, which corresponds to the condition where $\frac{d\Delta\beta(\lambda)}{d\lambda}$ approaches zero. In an analogous way, for the FSR_E of the Vernier envelope described by equation (8), the appearance of a UWL in the Vernier envelope requires the FSR_E to approach infinity within a specific wavelength region. This condition is satisfied when the FSRs of the sensing and reference interferometers become equal, i.e. FSR_S=FSR_R.

C. Comparative Analysis of Conventional Vernier Effect Schemes without FSR-Difference Zero Point and Proposed Single-Interferometer Vernier Schemes with FSR-Difference Zero Point

Based on the above analysis, the relationship between the FSRs of the sensing cell and the reference cell has further been investigated. Under the same simulation parameters as those used in the situation described in Fig. 1, the spectra of the two interferometers are shown in Fig. 2(a). Subsequently, the variation of the FSR with λ could then be obtained. Since the determination of the FSR relies on two adjacent wavelengths,

λ_1 and λ_2, the horizontal axis of the FSR scatter plot is represented by their average wavelength, $\lambda_{\bar{x}} = \frac{(\lambda_1+\lambda_2)}{2}$. As shown in Fig. 2(b), the FSR values are inherently discrete.

To facilitate further analysis, a linear fit has been performed to obtain a continuous FSR-λ curve. The fitted FSR-λ curves of the two interferometers are represented by the black and blue lines, respectively, in Fig. 2(c). It can be observed that, in a conventional Vernier effect scheme, the FSRs of both interferometers increase monotonically with wavelength. The FSR-difference curve, shown in Fig. 2(c), does not exhibit a zero point over the investigated wavelength range. As a result, no UWL appears in the output spectrum of the conventional Vernier effect, as illustrated in Fig. 1.

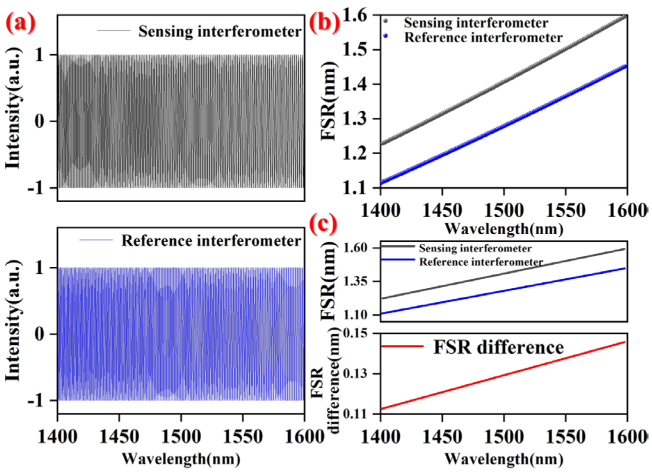

Fig. 2. (a) Spectra of the sensing interferometer and the reference interferometer. (b) Discrete FSR values as a function of wavelength. (c) Fitted FSR-λ curves and FSR-difference curve between the sensing and reference interferometers.

However, if the sensing spectrum is inverted along the wavelength axis at a specific central wavelength, the monotonicity of the FSR then is correspondingly reversed. Moreover, because the rate of change of the FSR with wavelength is typically small, the inverted spectrum naturally satisfies the FSR-matching condition required for the Vernier effect. Motivated by this observation, this work has proposed and then investigated a variable-period Vernier scheme that introduced a UWL into the Vernier envelope through single-interferometer spectral inversion, thereby enabling high-sensitivity dual-parameter sensing. Specifically, the sensing spectrum is inverted at the wavelength λ_0 along the wavelength axis to generate the reference spectrum, where λ_0 is defined as:

$$\lambda_0 = \frac{\lambda_{max} + \lambda_{min}}{2} \tag{9}$$

and where λ_{min} and λ_{max} respectively denote the minimum and maximum wavelengths of the spectral range. The intensity of the reference spectrum, I_R, can be expressed as:

$$I_R = cos\frac{4\pi n L_S}{2\lambda_0 - \lambda} \tag{10}$$

Numerical simulations have been performed to obtain the FSRs of the sensing and reference spectra, as well as their difference ΔFSR, as illustrated by the curves in Fig. 3(a). Owing to the spectral inversion, the FSRs of the sensing and reference interferometers are seen to exhibit a symmetric relationship, and the corresponding ΔFSR curve shows a zero point. For the parallel configuration of the two interferometers, the resulting output spectrum obtained is shown by the black curve in Fig. 3(b), where a clear UWL appears in the Vernier envelope. The wavelength of this UWL corresponds exactly to λ_0.

When the cavity length of the sensing cell changes in response to the measurand, the output spectra generated by the proposed scheme and their corresponding responses are shown in Fig. 3(b). It can be seen that the wavelength shift of the spectral peak closest to the UWL has significantly been enhanced, yielding a sensitivity improvement by a factor of 27, compared with that of the single sensing interferometer. Moreover, the intensity of the UWL also can be seen to vary with the measurand. Consequently, by simultaneously tracking the wavelength of a specific peak in the vicinity of the UWL and the intensity variation at the UWL, efficient dual-parameter measurement can be achieved.

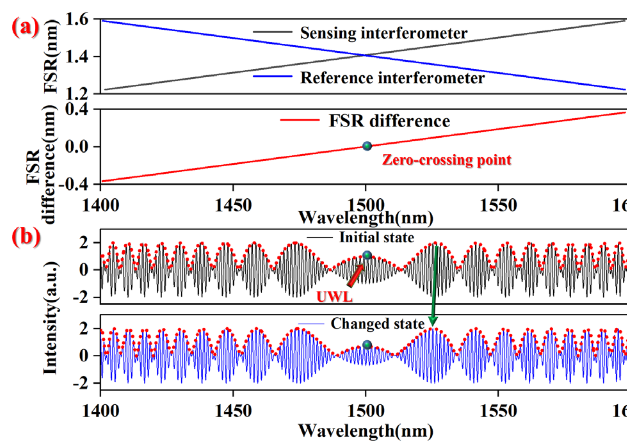

Fig. 3. (a) FSR-λ curves of the sensing and reference interferometers, and FSR-difference curve of the proposed scheme. (b) Output spectrum and its evolution under variation of the sensing interferometer.

III. Experimental Case and Discussion

A. Experimental Setup

Exploiting the advantages of a compact structure and ease of fabrication, a Fabry-Perot interferometer-based sensor has been fabricated as a representative example, to verify experimentally the scheme for simultaneous humidity and temperature measurement proposed in this work. The sensor was formed by fusion splicing a single mode fiber (SMF) with a hollow core fiber (HCF). A polyimide (PI) film was subsequently coated on the end face of the HCF to form the cavity. The sensing structure followed methods previously reported in the literature [23], [24], [25]. The thickness of the PI film was known to vary in response to ambient humidity and temperature changes, thereby modulating the effective cavity length of the sensor. As a result, the interferometric spectrum shifted accordingly, enabling the sensor to respond in a highly sensitive way to the external measurands considered.

An experimental setup designed for humidity and temperature measurements has been created and is schematically illustrated in Fig. 4. Here, the broadband super continuum light source (SLS, YSL Co. Ltd., SC-5) was employed to illuminate the sensor under test. The transmitted light from the sensor was subsequently guided to an Optical Spectrum Analyzer (OSA, Yokogawa, type AQ6370D), where the sensing spectra were recorded. During the experiment, the sensor was placed inside a commercial temperature-humidity chamber (THC, Binder, KBF 115), precisely to control and then monitor the ambient humidity and temperature conditions.

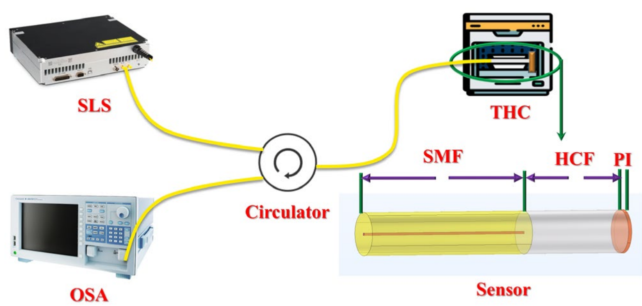

Fig. 4. Experimental setup used for the humidity and temperature measurements described. (SLS – Supercontinuum light source; THC – temperature-humidity chamber; OSA – Optical Spectrum Analyzer; SMF – single mode fiber; HCF – Hollow Core Fiber; PI – Polyimide film)

B. Humidity and Temperature Responses of the Single Sensing Interferometer

First, the humidity test was performed. Here, the spectra of the sensor, recorded by the OSA, were filtered and normalized as the humidity varied from 70 %RH to 50 %RH (with an interval of 5 %RH) while the temperature was maintained at 25 °C, and are shown in Fig. 5(a). It can be observed that the spectral peak near 1500 nm on the longer wavelength side exhibits a clear blue shift with decreasing humidity. The corresponding humidity sensitivity was calculated to be 18.8 pm/%RH, as seen from Fig. 5(b).

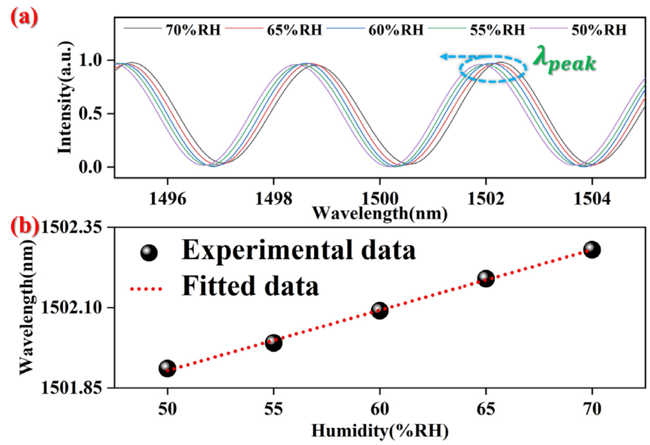

Fig. 5. (a) Normalized spectra of the single interferometric sensor as the humidity decreases from 70 %RH to 50 %RH. (b) Corresponding wavelength response as a function of humidity.

Subsequently, in the second phase of the experiment, the temperature response of the sensor was evaluated, at a fixed humidity of 50 %RH in the chamber. During this measurement, the temperature increased from 25 °C to 45 °C (with an interval of 5 °C), and the corresponding normalized spectra obtained are shown in Fig. 6(a). As the temperature increased, the spectral peak exhibited a red shift, showing a temperature sensitivity of 29.8 pm/°C.

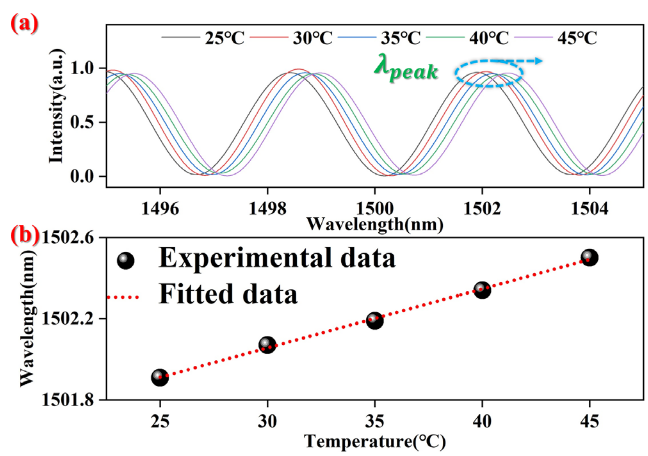

Fig. 6. (a) Normalized spectra of the single interferometric sensor as the temperature increases from 25 °C to 45 °C. (b) Corresponding wavelength response as a function of temperature.

C. Humidity and Temperature Responses of the Proposed Vernier Effect Sensor with UWL

Based on the theoretical analysis presented above, the corresponding reference spectra were generated by inverting the sensing spectra along the wavelength axis. The central wavelength, λ_0, was determined to be 1500 nm, and the inverted reference spectra corresponding to the humidity-dependent sensing spectra in Fig. 5(a) are shown in Fig. 7.

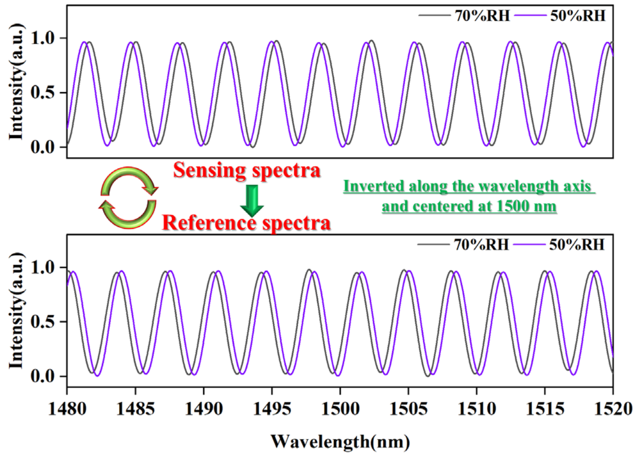

Fig. 7. Inverted reference spectra generated from the sensing spectra under humidity variations.

To enhance the sensitivity and also enable dual-parameter measurement, the proposed Vernier effect scheme was implemented by superimposing the sensing spectra upon the corresponding inverted reference spectra. The resulting output spectra, obtained under different humidity conditions, can be seen in Fig. 8(a). UWL emerges at the central wavelength, this being clearly distinguishable from the periodic envelope observed in the conventional Vernier envelope.

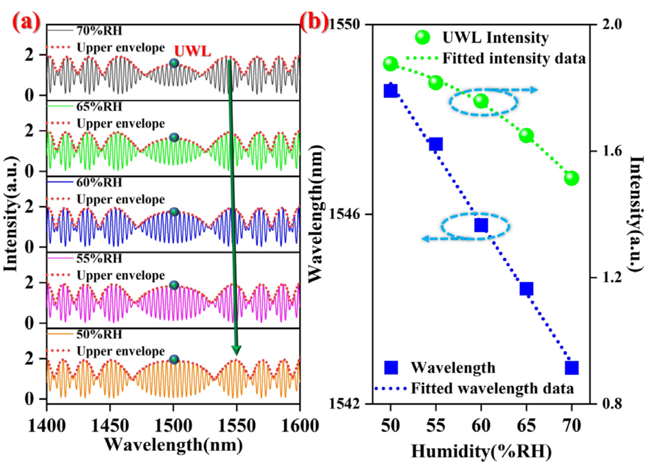

Fig. 8. (a) Spectra of the proposed Vernier effect-based sensor with a UWL as the humidity decreases from 70 %RH to 50 %RH. (b) Wavelength shift and the intensity variation of the UWL versus humidity.

The wavelength shift of the spectral peak nearest to the UWL on the longer-wavelength side exhibits a high sensitivity of -294.6 pm/%RH (R^2=0.994), representing an approximately sixteen fold enhancement compared with that of the single sensing interferometer (presented in Fig. 5). In addition, the intensity at the UWL varies monotonically with humidity. The wavelength shift of the peak and the corresponding intensity variation at the UWL, obtained as functions of humidity, are shown in Fig. 8(b). The corresponding wavelength of the peak, denoted as λ_{Peak_RH} and the corresponding intensity at the UWL, denoted as I_{UWL_RH}, can be expressed as follows:

$$\begin{aligned} \lambda_{Peak\_RH} &= -0.294 * RH + 1563.484 \\ I_{UWL\_RH} &= -0.000578 * RH^2 + 0.0516 * RH + 0.738 \end{aligned} \quad (11)$$

Similarly, the output spectra of the Vernier effect sensor proposed in this work, monitored under varying temperature conditions, are shown in Fig. 9(a). The spectral peak closest to the UWL demonstrates a temperature sensitivity of -519.6 pm/°C (R^2=0.985), corresponding to an approximately seventeen fold increase relative to that of the single sensing interferometer (presented in Fig. 6). Moreover, the intensity at the UWL changes monotonically with temperature. The wavelength shift of the selected peak and the corresponding intensity variation at the UWL, as functions of temperature, are presented in Fig. 9(b).

The corresponding wavelength of the peak, denoted as λ_{Peak_T} and the corresponding intensity at the UWL, denoted as I_{UWL_T}, can be expressed as shown below, where:

$$\begin{aligned} \lambda_{Peak\_T} &= -0.520 * T + 1561.978 \\ I_{UWL\_T} &= -0.000728 * T^2 + 0.0169 * T + 1.920 \end{aligned} \quad (12)$$

Based on the distinctive response characteristics of the wavelength shift and the intensity variation at the UWL to changes in humidity and temperature, the proposed Vernier effect not only provides substantial sensitivity enhancement but also produces distinct and separable responses, enabling reliable and effective dual-parameter discrimination. The two measurands can be simultaneously determined by jointly solving equation (11) and equation (12), following principles similar to those reported in the literature [26], [27]. Five repeated experiments were conducted with simultaneous variations of both parameters. The maximum errors between the calculated and true values were 0.83 °C for temperature and 1.78 %RH for humidity.

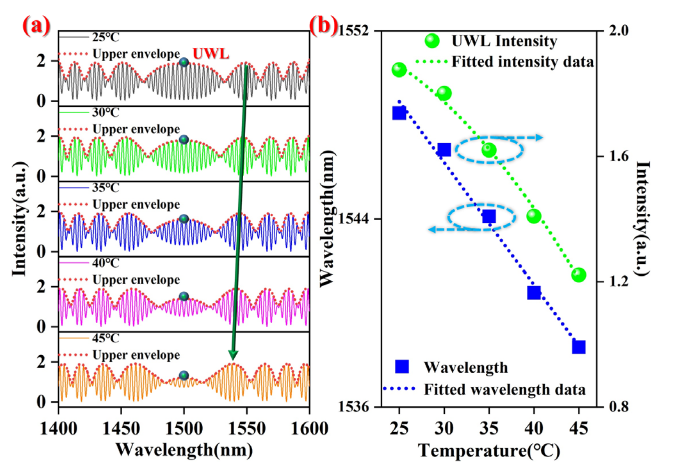

Fig. 9. (a) Spectra of the proposed Vernier effect-based sensor with a UWL as the temperature increases from 25 °C to 45 °C. (b) Wavelength shift and the intensity variation of the UWL versus temperature.

To evaluate the long-term stability and resolution of the system, five repeated measurements were performed under constant temperature and humidity conditions [28]. The maximum wavelength fluctuations were 0.667 nm and 0.584 nm for humidity and temperature, respectively. Based on these fluctuations, the corresponding resolutions were estimated to be 2.26 %RH for humidity and 1.28 °C for temperature.

However, the UWL intensity exhibits a periodic response arising from the superposition of the outputs of the two interferometers with periodic spectral characteristics, which limits the unambiguous measurement range to one period under intensity-based interrogation. Moreover, intensity readout is inherently more susceptible to noise. These limitations may be mitigated in future work by introducing wavelength references (e.g., FBGs) or by combining multi-peak interrogation schemes that exploit differential sensitivities (e.g., the first and second peaks near UWL on the longer wavelength side).

IV. Conclusion

In summary, this paper has shown, for the first time, the success of an investigation into the equal FSR critical condition of the Vernier effect. In this work, by introducing a deliberately designed spectral inversion scheme in which the sensing interferometer spectrum is inverted to form the reference spectrum, both the FSR matching condition and the equal FSR condition have been satisfied. Under these critical conditions, a UWL emerges in the Vernier envelope, at a specific wavelength. The presence of the UWL thus provides a stable and distinguishable spectral feature, effectively overcoming the inherent periodic ambiguity of the conventional Vernier effect sensors in long-term and continuous measurement. Moreover, by jointly exploiting the intensity variation at the UWL and the enhanced wavelength shift of a specific peak or dip in its vicinity, reliable dual-parameter sensing, importantly with significantly improved sensitivity, has been achieved. As a result, this work has clearly established a clear link between the equal FSR critical condition and the formation of a UWL in the Vernier envelope. The concept proposed herein can be seen to open a promising avenue for the development of high-performance and multi-parameter optical fiber sensors, important for use by industry.

References

[1] A.D. Gomes, H. Bartelt, and O. Frazao, “Optical Vernier effect: Recent advances and developments,” *Laser Photon. Rev.*, vol. 15, p. 2000588, 2021.

[2] Y.X. Liu, X.G. Li, Y.N. Zhang, and Y. Zhao, “Fiber-optic sensors based on Vernier effect,” *Measurement*, vol. 167, p. 108451, 2021.

[3] W. Naku, J. Huang, and C. Zhu, “Optical fiber sensors based on advanced Vernier effect: A review,” *IEEE Sensors J.*, vol. 24, no. 9, pp. 13758-13772, 2024.

[4] Z. Li , Y.X. Zhang , W.G. Zhang , L.X. Kong , and T.Y. Yan et al., “High-Sensitivity Gas Pressure Fabry-Perot Fiber Probe With Micro-Channel Based on Vernier Effect,” *J. Lightw. Technol.*, vol. 37, no. 14, pp. 3444-3451, 2019.

[5] Q. Chen, Z.Y. Zhang, J.B. Bao, Y. Cai, and Yong Zhao, “Vernier-effect-enhanced FPI optical fiber sensor for ultrasensitive Cu2 + detection,” *Sens. Actuators B Chem.*, vol. 450, p. 139214, 2026.

[6] X.M. Yang, S. Wu, H.H. Cheng, J.W. Ma, and S. Wang et al., “Simplified highly-sensitive gas pressure sensor based on harmonic Vernier effect,” *Opt. Laser Technol.*, vol. 140, p. 107007, 2021.

[7] X.G. Li , F. Li , X. Zhou , Y.N. Zhang , and L.V. Nguyen et al., “Optical Fiber DNA Biosensor With Temperature Monitoring Based on Double Microcavities Fabry-Perot Interference and Vernier Combined Effect,” *IEEE Trans. Instrum. Meas.*, vol. 72, pp. 1-8, 2023.

[8] F. Li, X.G. Li, X. Zhou, P.Q. Gong, and Y.N. Zhang et al., “Plug-in label-free optical fiber DNA hybridization sensor based on C-type fiber Vernier effect,” *Sens. Actuators B Chem.*, vol. 354, p. 131212, 2022.

[9] X.G. Hu, Z.K. Li, J.W. Zhang, X.X. Wang, and X.M. Chen et al., “In-situ label-free optofluidic DNA biosensor based on fiber-optic Michelson interferometer with vernier effect for microfluidic chip,” *Measurement*, vol. 254, p. 117973, 2025.

[10] Y. Wang, W.H. Yuan, Y.X. Yan, Z.G. Lian, and D.R. Chen *et al.*, “Signal processing integrated with fiber-optic Vernier effect for the simultaneous measurement of relative humidity and temperature,” *Opt. Exp.*, vol. 31, no. 17, pp. 28636-28648, 2023.

[11] R.J. Tong, B. Xing, Z.H. Chen, H.N. Zheng and L.M. Zhou, “High-Sensitivity Fiber Optic Temperature Sensor Based on Enhanced Vernier Effect,” *IEEE Trans. Instrum. Meas.*, vol. 73, pp. 1-8, 2024.

[12] C.G. Yu, H.P. Gong, Z.X. Zhang, K. Ni and C.L. Zhao, “Temperature-compensated high-sensitivity relative humidity sensor based on band-pass filtering and Vernier effect,” *IEEE Trans. Instrum. Meas.*, vol. 71, pp. 1-8, 2022.

[13] A. Zornoza, J. A. Flores-Bravo, J. Zubia, and J. Villatoro, “Sensitivity magnification of an interferometric optical fiber sensor with a length-linked virtual reference,” *Opt. Laser Technol.*, vol. 167, p. 109819, 2023.

[14] G.X. Bei, T. Wei, H.L. Ma, L.Q. Zhang, Y.C. Yao, M.H. Wang, J.H. Yuan, and Q. Wu, “Combination of virtual optical Vernier method and peak position recognition without envelope fitting: A general method for sensor sensitivity enhancement,” *J. Lightw. Technol.*, vol. 43, no. 7, pp. 3292-3299, 2025.

[15] Y.Q. Guan and X.P. Dong, “Sensitivity-enhanced flow rate sensor based on Vernier effect with a virtual reference cell,” *IEEE Sensors J.*, vol. 22, no. 24, pp. 23915-23922, 2022.

[16] Y.Q. Guan, M. Fabian, H.W. Gao, Y.B. Feng, and X.P. Dong *et al.*, “Highly sensitive humidity measurement with temperature compensation based on a special dual-modal interferometric sensor and varied period Vernier effect,” *IEEE Sensors J.*, vol. 24, no. 7, pp. 10172-10179, 2024.

[17] C.X. Lu, X.P. Dong, L.H. Lu, Y.Q. Guan and S.Q. Ding, “Label free all-fiber static pressure sensor based on Vernier effect with temperature compensation,” *IEEE Sensors J.*, vol. 20, no. 9, pp. 4726-4731, 2020.

[18] C.X. Lu, J. Su, X.P. Dong, T. Sun and K. T. V. Grattan, “Simultaneous Measurement of Strain and Temperature With a Few-Mode Fiber-Based Sensor,” *J. Lightw. Technol.*, vol. 36, no. 13, pp. 2796-2802, 2018.

[19] C.X. Lu, J. Su, X.P. Dong, L.H. Lu, T. Sun and K. T. V. Grattan *et al.*, “Studies on Temperature and Strain Sensitivities of a Few-mode Critical Wavelength Fiber Optic Sensor,” *IEEE Sensors J.*, vol. 19, no. 5, pp. 1794-1801, 2019.

[20] X. Lei, X. Dong, C. Lu, T. Sun and K. T. V. Grattan, “Underwater Pressure and Temperature Sensor Based on a Special Dual-Mode Optical Fiber,” *IEEE Access*, vol. 8, pp. 146463-146471, 2020.

[21] Y. Liu, R. Zhou, X. Xu, R. Li and F. Li, “Sensitivity Enhanced Fiber-Optic Hydrogen Sensor Based on Vernier Effect of Polymer–Air Cascaded FPI,” *IEEE Sensors J.*, vol. 25, no. 6, pp. 9626-9632, 2025.

[22] A.D. Gomes, M.S. Ferreira, J. Bierlich, J. Kobelke, and M. Rothhardt et al., “Optical harmonic Vernier effect: a new tool for high performance interferometric fiber sensors,” *Sensors*, vol. 19, no. 24, p. 5431, 2019.

[23] Y. Wang, Q. Huang, W. Zhu and M. Yang, “Simultaneous Measurement of Temperature and Relative Humidity Based on FBG and FP Interferometer,” *IEEE Photonics Technol. Lett.*, vol. 30, no. 9, pp. 833-836, 2018.

[24] Y.S. Zhong, P.B. Xu, J. Yang, and X.Y. Dong, “Optical Fiber Interferometric Humidity Sensor by Using Hollow Core Fiber Interacting with Gelatin Film,” *Sensors*, vol. 22, no. 12, p. 4514, 2022.

[25] G.L. Zhang, M.H. Yang, and M. Wang, “Large temperature sensitivity of fiber-optic extrinsic Fabry-Perot interferometer based on polymer-filled glass capillary,” *Opt. Fiber Technol.*, vol. 19, no. 6, pp. 618-622, 2013.

[26] A. Urrutia, J. Goicoechea, A.L. Ricchiuti, D. Barrera, and S. Sales *et al.*, “Simultaneous measurement of humidity and temperature based on a partially coated optical fiber long period grating,” *Sens. Actuators B Chem.*, vol. 227, pp. 135-141, 2016.

[27] Y.T. Bai, Y.P. Miao, H.M. Zhang, and J.Q. Yao. “Simultaneous measurement of temperature and relative humidity based on a microfiber Sagnac loop and MoS2,” *J. Lightw. Technol.*, vol. 38, no. 4, pp. 840-845, 2020.

[28] C. Zhou, J.J. Tian, and Y. Yao, “Hybrid Vernier effect: sensitivity amplification and two-parameter measurement in cascaded Fabry-Perot interferometer fiber sensor,” *Opt. Exp.*, vol. 31, pp. 41701-41712, 2023.